Title: Impact of the chain length and topology of the acetylated oligosaccharide on the crystallization tendency of naproxen from amorphous binary mixtures

Author: Aldona Minecka, Magdalena Tarnacka, Karolina Jurkiewicz, Barbara Hachuła, Roman Wrzalik, Kamil Kamiński (i in.)

Citation style: Aldona Minecka, Magdalena Tarnacka, Karolina Jurkiewicz, Barbara Hachuła, Roman Wrzalik, Kamil Kamiński (i in.). (2021). Impact of the chain length and topology of the acetylated oligosaccharide on the crystallization tendency of naproxen from amorphous binary mixtures. "Molecular Pharmaceutics" (2021) iss. 1, s. 347-358. DOI: 10.1021/acs.molpharmaceut.0c00982

molecular pharmaceutics

pubs.acs.org/molecularpharmaceutics

Article

Impact of the Chain Length and Topology of the Acetylated Oligosaccharide on the Crystallization Tendency of Naproxen from Amorphous Binary Mixtures

Aldona Minecka,* Magdalena Tarnacka, Karolina Jurkiewicz, Barbara Hachuła, Roman Wrzalik, Kamil Kamiński, Marian Paluch, and Ewa Kamińska*

Cite This: *Mol. Pharmaceutics* 2021, 18, 347−358

Read Online

ACCESS | Metrics & More | Article Recommendations | Supporting Information

ABSTRACT: The impact of the chain length or dispersity of polymers in controlling the crystallization of amorphous active pharmaceutical ingredients (APIs) has been discussed for a long time. However, because of the weak control of these parameters in the majority of macromolecules used in pharmaceutical formulations, the abovementioned topic is poorly understood. Herein, four acetylated oligosaccharides, maltose (acMAL), raffinose (acRAF), stachyose (acSTA), and α-cyclodextrin (ac-α-CD) of growing chain lengths and different topologies (linear *vs* cyclic), mimicking the growing backbone of the polymer, were selected to probe the influence of these structural factors on the crystallization of naproxen (NAP)—an API that does not vitrify regardless of the cooling rate applied in our experiment. It was found that in equimolar systems composed of NAP and linear acetylated oligosaccharides, the progress and activation barrier for crystallization are dependent on the molecular weight of the excipient despite the fact that results of Fourier transform infrared studies indicated that there is no difference in the interaction pattern between measured samples. On the other hand, complementary dielectric, calorimetric, and X-ray diffraction data clearly demonstrated that NAP mixed with ac-α-CD (cyclic saccharide) does not tend to crystallize even in the system with a much higher content of APIs. To explain this interesting finding, we have carried out further density functional theory computations, which revealed that incorporation of NAP into the cavity of ac-α-CD is hardly possible because this state is of much higher energy (up to 80 kJ/mol) with respect to the one where the API is located outside of the saccharide torus. Hence, although at the moment, it is very difficult to explain the much stronger impact of the cyclic saccharide on the suppression of crystallization and enhanced stability of NAP with respect to the linear carbohydrates, our studies clearly showed that the chain length and the topology of the excipient play a significant role in controlling the crystallization of this API.

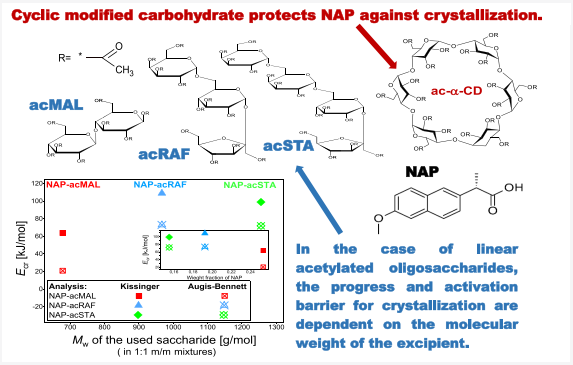

KEYWORDS: *naproxen, acetylated saccharides, binary mixtures, chain length, topology, crystallization tendency*

INTRODUCTION

Polymers are the most popular and universal excipients (EXCs) in the pharmaceutical industry. They are employed as carriers, solubilizers, dispersive agents, emulsifiers, dissolution-retarding agents, coating substances, media for semiliquid forms of drugs, parts of various therapeutic systems, and so forth.[1−3] Macromolecules (of varying masses and internal configurations) commonly used in formulation technology include polysiloxanes, polyvinyl caprolactam−polyvinyl acetate−polyethylene glycol graft copolymer (Soluplus), hypromellose (HPMC), hypromellose acetate succinate (HPMCAS), poly(ethylene glycol) (PEG), polyoxyethyleneglycols, polyvinylpyrrolidone (PVP), and PVA/vinyl acetate (PVP/VA). It is worth mentioning that these widely known and accepted by Food and Drug Administration (FDA) and European Medicines Agency (EMA) substances became a very important class of materials that can be used as long-term stabilizers of labile amorphous active pharmaceutical ingredients (APIs), whose apparent solubility and hence bioavailability are more beneficial in comparison to those of their crystalline counterparts. Recent studies have revealed that the abovementioned polymers (i) are physically and chemically stable in a wide range of pressures (p) and temperatures (T), (ii) easily form binary mixtures with different kinds of disordered pharmaceuticals, and (iii) have a strong influence

Received: September 30, 2020
Revised: December 1, 2020
Accepted: December 7, 2020
Published: December 23, 2020

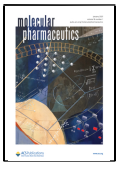

Scheme 1. Chemical Structures of NAP and Acetylated Saccharides Used to Prepare Binary Mixtures: acMAL, acRAF, acSTA, and Acetylated α-Cyclodextrin (ac-α-CD)

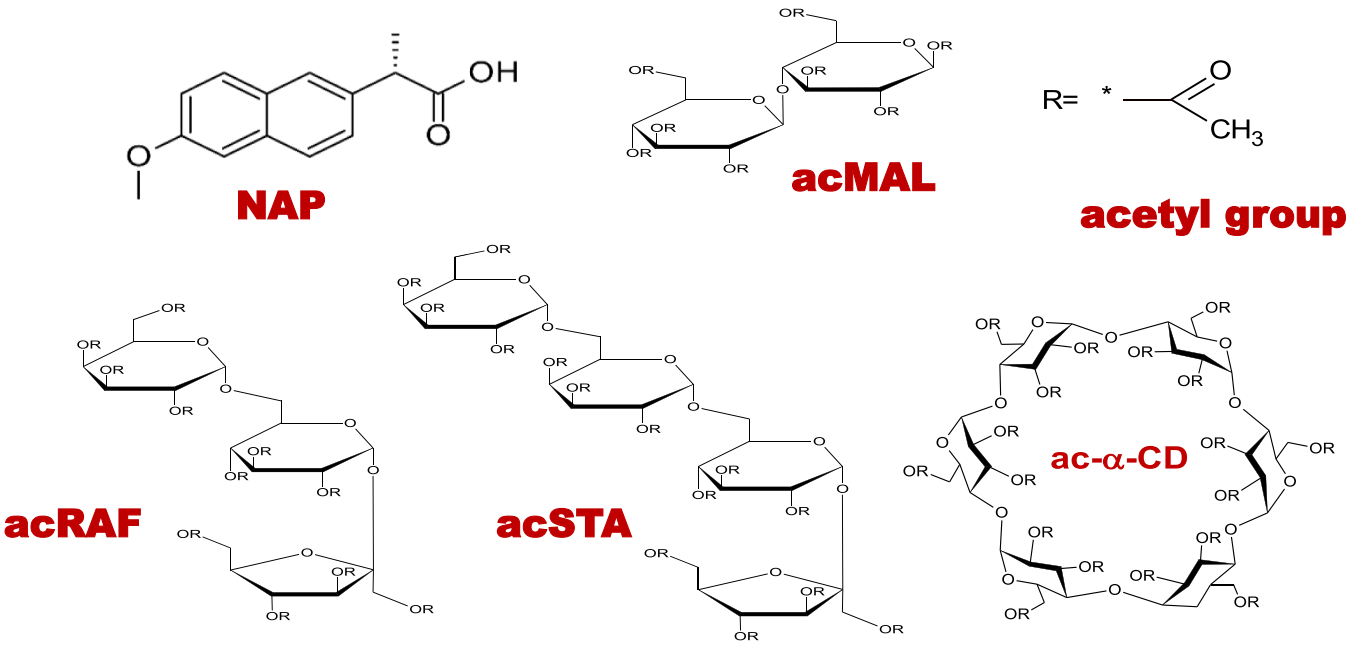

on the dissolution rates, solubility of active substances, and so forth.[4,5] Until now, stable amorphous API−polymer systems have been created, for example, for ezetimibe,[6] nimesulide,[7] bicalutamide,[8] flutamide,[9] tadalafil,[10] nabumetone,[11] naproxen (NAP),[12] indomethacin,[13] sulfonamide,[14] celecoxib,[15,16] nifedipine,[17] or furosemide.[18] Interestingly, some of them (e.g., mixtures with griseofulvin (Gris-PEG), fenofibrate (FENOGLIDE), itraconazole (SPORANOX), verapamil hydrochloride (Isoptin), and lopinavir−ritonavir (KALETRA)) are even available on the market.[4,19−21] Unfortunately, despite the indicated favorable properties, commercial polymers have significant disadvantages. First of all, these systems are often not well characterized from the chemical/molecular point of view. In many cases, the molar mass and dispersity, which defines the degree of heterogeneous chain length distribution, are poorly controlled. The most illustrative examples are PVP or derivatives of polysaccharides, where either dispersity of the polymer is very high or degree of substitution of hydroxyl units is not well defined. These deficiencies connected to weak control of the basic properties of macromolecules may have significant implications on the homogeneity and stability of the prepared drug formulations. As a consequence, a risk of phase microseparation, often leading to enhanced crystallization and changing the dissolution properties over the time of storage, increases markedly. Moreover, the research done in previous years on the very poorly characterized polymers seems to be a limiting step in better understanding the role of the chain length, the flexibility of the polymer backbone, or its topology in the stability of amorphous (and easily crystallizing) pharmaceuticals.

Taking into account the abovementioned problem, the interesting alternatives for polymers are low-molecular weight EXCs. Among them, amino acids,[22−25] small proteins,[26,27] organic acids,[28] other active substances,[29−31] and carbohydrates and their modified analogues[32−38] (prepared by substituting the hydrogen atom from hydroxyl groups by hydrophobic, e.g., acetyl moieties) are commonly applied to stabilize amorphous APIs. From the mentioned groups, saccharides deserve special attention. Note that these are nontoxic and biocompatible systems (many of them are accepted by the FDA and EMA as food and drug additives). Moreover, because of chemical modification, it is possible to tune their physicochemical properties. Indeed, substituted carbohydrates are free from limitations characteristic for polymers (dispersity problem) and amino acids (thermodegradation). Moreover, they improve the solubility of APIs belonging to the II and IV class of the Biopharmaceutics Classification System (BCS). It is also worth adding that these compounds are often characterized by high glass transition temperature, T_g (consequently, the stability of their binary mixtures with APIs at room temperature is greater), and they can easily be transformed to the amorphous state via vitrification, which is the simplest method of producing glasses. It is just mentioned that acetylated derivatives of some mono- and disaccharides have been recently used to stabilize amorphous forms of indomethacin,[32] nifedipine,[34] furosemide,[35] itraconazole,[36] NAP,[37] celecoxib,[33] and bicalutamol.[38] Unfortunately, besides these investigations, there are no similar reports on the binary mixtures composed of APIs and carbohydrates (e.g., oligosaccharides) with more complex architectures/topologies. Importantly, such saccharides, whose basic structural units are glucose, galactose, and fructose, can form linear chains (with various lengths) or cyclic structures. Therefore, they seem to be convenient models to simulate simple, small-scale polymeric systems. Consequently, research on API−oligosaccharide mixtures would certainly help us to answer the question (impossible or hard to resolve in the case of polymers)—how the length and topology of the matrix influence the glass-forming ability and stability/crystallization tendency of amorphous APIs.

In this paper, four modified saccharides with linear or cyclic structures: acetylated maltose (acMAL), acetylated raffinose (acRAF), acetylated stachyose (acSTA), and acetylated-α-cyclodextrin (ac-α-CD) have been used to prepare amorphous

https://dx.doi.org/10.1021/acs.molpharmaceut.0c00982
Mol. Pharmaceutics 2021, 18, 347−358

binary mixtures with NAP—a popular nonsteroidal anti-inflammatory drug (NSAID), which cannot be prepared in the glassy state via vitrification because of its strong tendency for crystallization. Our purpose was to answer the question whether both the topology and length of the saccharide chain have a significant role in suppressing the crystallization of the considered pharmaceutical.

EXPERIMENTAL SECTION

Materials and Methods. *Materials.* NAP ([IUPAC name: (2S)-2-(6-methoxy-2-naphthyl)propanoic acid], $C_{14}H_{14}O_3$, M_w = 230.3 g/mol, 99% purity) was supplied by TCI Europe. acMAL (octaacetylmaltose, $C_{28}H_{38}O_{19}$, M_w = 678.6 g/mol, 98% purity) was provided by Sigma-Aldrich. acRAF (undecaacetylraffinose, $C_{40}H_{54}O_{27}$, M_w = 966.9 g/mol, 99% purity), acSTA (tetradecaacetylstachyose, $C_{52}H_{70}O_{35}$, M_w = 1255.3 g/mol, 99% purity), and ac-α-CD (octadecaacetyl-α-cyclodextrin, $C_{72}H_{96}O_{48}$, M_w = 1729.7 g/mol, 99% purity) were synthesized for the purpose of this paper. The synthesis procedures (including NMR data of the obtained products) are presented in the Supporting Information in ref 39. The molecular structures of all investigated compounds are presented in Scheme 1. Note that acMAL is a disaccharide, which consists of two glucose units; acRAF is a trisaccharide composed of galactose, glucose, and fructose, while acSTA is a tetrasaccharide consisting of two galactose units, one glucose unit and one fructose unit. ac-α-CD is a cyclic hexasaccharide composed of six glucose monomers. In all examined carbohydrates, the hydrogen atoms from hydroxyl groups are substituted by acetyl moieties.

Methods. Preparation of Binary Systems of NAP with Modified Saccharides. The amorphous binary mixtures of NAP with four selected acetylated oligosaccharides (molar ratios: 10:1, 5:1, 3:1, 2:1, 1:1, 1:3, 1:5, and 1:10) were prepared using the quench cooling technique in a temperature- and humidity-controlled glovebox (PLAS Laboratories Inc. 890-THC-DT/EXP/SP) at the assured relative humidity RH < 10%. To obtain the homogeneous solid dispersions (SDs), we first mixed NAP with EXCs (all substances were the white crystalline powders) in a heat-resistant glass vial and subsequently put a magnetic stir bar into the vial with the mixtures. Next, the crystalline components were melted in the vial on the hot plate magnetic stirrer (CAT M 17.5 with the Pt-100 temperature sensor) at T slightly above the T_m of NAP (~435 K). After the full melting of the prepared binary systems, they were transferred from the hot metal plate to a very cold ($T \sim 278$ K) metal plate with the applied cooling rate of ~ 100 K/min (the given value is just a rough estimation using the contact thermometer). The supercooled samples obtained in this way were further analyzed with the use of differential scanning calorimetry (DSC) and broadband dielectric spectroscopy (BDS). Because of the fact that these investigations clearly revealed enhanced crystallization/phase separation in the mixtures (NAP−acMAL, NAP−acRAF, and NAP−acSTA) with the higher content of APIs (10:1, 5:1, 3:1, and 2:1 m/m) and good physical stability (no sign of crystallization) of the systems with the greater amount of modified oligosaccharides (1:3, 1:5, and 1:10 m/m), further nonisothermal DSC, X-ray diffraction (XRD), and Fourier transform infrared spectroscopy (FTIR) measurements were carried out exclusively on equimolar, 1:1 m/m, mixtures—optimal molar ratio (for nonisothermal DSC studies also, 1:5.45 w/w systems were prepared). Note that in the case of the NAP−ac-α-CD system, despite the stability of APIs in each prepared sample (as concluded from BDS and DSC studies), additional XRD and FTIR experiments were also performed on the 1:1 m/m mixture.

Differential Scanning Calorimetry. Calorimetric measurements of mixtures of NAP with acetylated saccharides were performed using a Mettler Toledo DSC apparatus (Mettler Toledo International, Inc., Greifensee, Switzerland) calibrated for temperature and enthalpy using indium and zinc standards and equipped with a liquid nitrogen cooling accessory and an HSS8 ceramic sensor (a heat flux sensor with 120 thermocouples). The studied binary systems were contained in sealed aluminum crucibles (40 μL) and heated above their melting temperatures, quenched, and scanned well above the respective melting points.

Nonisothermal calorimetric measurements (heating rates from 2.5 to 20 K/min) were carried out on equimolar (1:1 m/m) and 1:5.45 w/w NAP−acMAL, NAP−acRAF, and NAP−acSTA SDs, immediately after the preparation of amorphous samples. For each experiment, a fresh sample was prepared.

Broadband Dielectric Spectroscopy. Complex dielectric permittivity ($\varepsilon^*(\omega) = \varepsilon'(\omega) - i\varepsilon''(\omega)$) measurements were carried out using the Novocontrol Alpha dielectric spectrometer (Novocontrol Technologies GmbH & Co. KG, Hundsangen, Germany) over the frequency range from 10^{-2} to 10^6 Hz. Experiments were performed after the vitrification process (which was described above) at ambient pressure in a broad range of temperatures (299−445 K). The samples were placed between two stainless-steel flat electrodes of the capacitor with a gap of 0.1 mm, mounted in a cryostat, and kept under dry nitrogen gas flow during measurements. The temperature stability controlled using a Quatro cryosystem using a nitrogen gas cryostat was better than 0.1 K.

X-Ray Diffraction. XRD measurements for neat crystalline NAP,supercooled acetylated saccharides and their equimolar binary mixtures were performed on a Rigaku-Denki D/MAX RAPID II-R diffractometer equipped with a rotating Ag anode, a graphite (002) monochromator, and an image plate detector in the Debye−Scherrer geometry. The wavelength of the incident beam was 0.56 Å. Samples were measured just after the preparation in borosilicate glass capillaries at 293 K. The background intensity from the empty capillary was subtracted, and two-dimensional diffraction patterns were converted into one-dimensional intensity data *versus* the scattering angle, 2θ.

Fourier Transform Infrared Spectroscopy. Infrared experiments were carried out with a Thermo Scientific Nicolet iS50 FT-IR spectrometer using a diamond attenuated total reflection accessory. The data were recorded in the range of 4000−400 cm^{-1} by averaging 32 scans at a resolution of 4 cm^{-1}. FTIR spectra of carbon tetrachloride (CCl_4) and NAP diluted in CCl_4 were also measured on a Nicolet iS50 FTIR spectrometer in the frequency range from 4000 to 400 cm^{-1} using a transmission solution cell with KBr windows and a path length of 1.03 mm. A total of 16 scans with a spectral resolution of 4 cm^{-1} were averaged for each sample. The IR spectrum of NAP solution was obtained by subtracting the spectrum of the pure solvent (CCl_4) from the measured absorption spectrum and by applying baseline correction.

Density Functional Theory Calculations. Full optimization of the molecular structure of the isolated α-cyclodextrin (nonmodified) molecule and its acetyl derivative (ac-α-CD) and NAP (S-form) was carried out with the density functional

https://dx.doi.org/10.1021/acs.molpharmaceut.0c00982
Mol. Pharmaceutics 2021, 18, 347−358

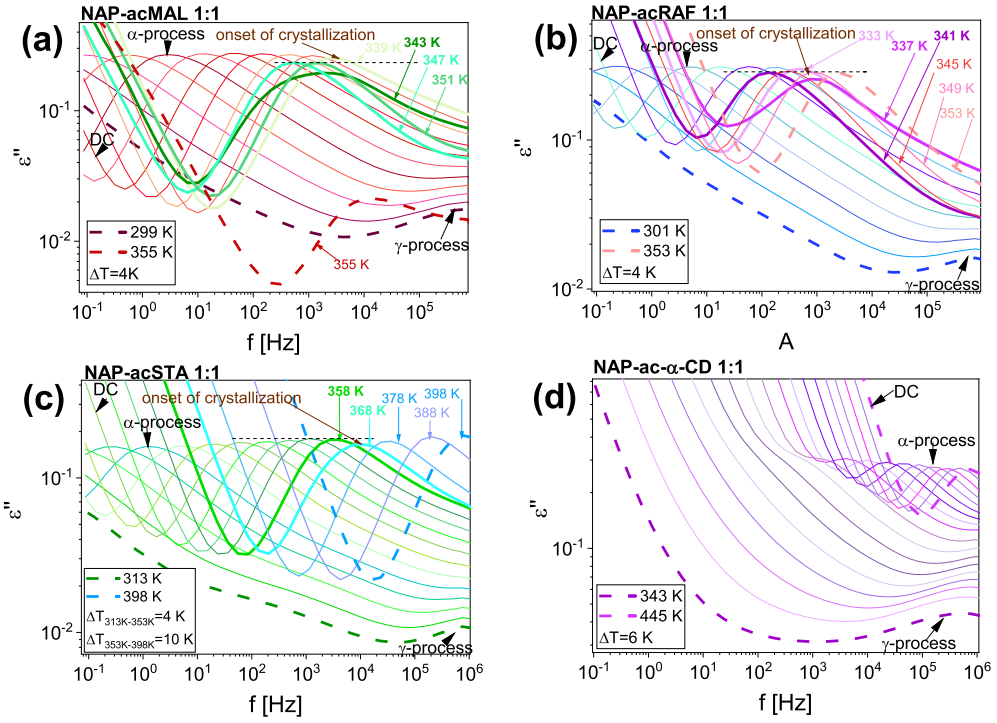

Figure 1. Representative dielectric loss spectra measured above T_g for equimolar binary mixtures of NAP with acMAL, acRAF, acSTA, and ac-α-CD. The thickened lines were used to show the changes in the amplitude of the α-peak due to crystallization.

theory (DFT) B3LYP/6-31G(d) model using Gaussian 03 software.[40]

RESULTS AND DISCUSSION

At the beginning, it should be stressed that to study the impact of the chain length and topology (linear *vs* cyclic) of acetylated saccharides (acSACCHs) on the crystallization tendency of NAP, first, we have prepared binary mixtures with various contents of a given EXC. Next, preliminary DSC and BDS measurements were performed on each system. The purpose of these experiments was to find out an optimal concentration of acSACCHs, at which the crystallization of the considered API is neither too fast nor too slow. It turned out that the mixtures of NAP with acMAL (disaccharide), acRAF (trisaccharide), and acSTA (tetrasaccharide) prepared in 3:1 and 2:1 molar ratios m/m (and with a lower EXC content) are highly unstable. Namely, in a very short time after the sample preparation, we observed the crystallization and phase separation manifested, dependently on the applied experimental technique, by clear exothermic events in thermograms or broadening of the α-relaxation peak and lowering of its amplitude in dielectric spectra. In turn, for the mixtures with the relatively large amount of modified linear oligosaccharide with respect to the API (1:3, 1:5, and 1:10 m/m), none of these behaviors were detected. Such systems were physically stable, and hence, the influence of the EXC on the crystallization of NAP could not be examined on the reasonable experimental time scale. An optimal molar ratio of NAP and acMAL (acRAF and acSTA) at which the mixtures were homogeneous and did not crystallize shortly after preparation was 1:1 m/m. Therefore, in further investigations, we focused only on these equimolar SDs. Simultaneously, one can mention that the mixtures of NAP with cyclic hexasaccharide (ac-α-CD) prepared in each molar ratio (even in 10:1 m/m) were stable, and no sign of crystallization and phase separation was noticed. Nevertheless, to retain consistency and clarity of further discussion, in this paper, we showed the results obtained exclusively for the NAP−ac-α-CD, 1:1 m/m binary system.

At first, the outcomes of BDS investigations will be presented. In Figure 1, representative dielectric loss spectra measured above the T_g for the considered SDs (1:1 m/m) are displayed. Note that dielectric spectra of neat modified saccharides (acMAL, acRAF, acSTA, and ac-α-CD) can be found in our recent papers (refs 36, 39). As can be seen, in the case of all mixtures, two well-visible processes, which shift toward lower frequencies (f) with decreasing temperature, can be detected. The first one is the dc conductivity (DC) connected to the charge transport of ionic impurities in the sample, whereas the second one is the structural relaxation (α), related to cooperative motions of molecules. Moreover, at lower T, there is a trace of secondary (γ)-relaxation, which originates from the motions of acetyl moieties.[39] It is worth noting that in the mixture of NAP with ac-α-CD (panel d), the impact of DC is very strong. As a consequence, with decreasing temperature, the low frequency side of the α-peak is systematically covered by DC contribution until complete obscuration. From Figure 1, it is also well seen that in contrast to the NAP−ac-α-CD system, for NAP−acMAL, NAP−acRAF, and NAP−acSTA, 1:1 m/m mixtures, the amplitude of the α-peak is lower at higher T. This behavior is accompanied by the broadening of α-dispersion. Interestingly, for the SDs with acMAL and acRAF, after the mentioned drop in the amplitude, the α-process is also shifting back toward lower f with increasing T. This unexpected finding indicates that the T_g of binary systems starts to increase. The reason for that is the decreasing content of amorphous NAP (a component with lower T_g in comparison to the modified saccharide) because of ongoing crystallization. What is more, with a further increase in the temperature, the α-peak moves

https://dx.doi.org/10.1021/acs.molpharmaceut.0c00982
Mol. Pharmaceutics 2021, 18, 347−358

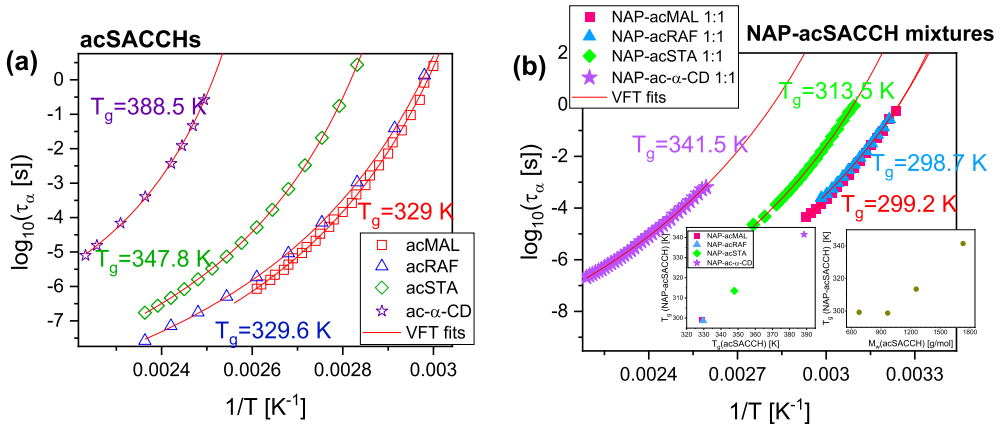

Figure 2. Structural (α) relaxation times plotted *vs* inverse temperature for neat acetylated saccharides[36,39] (a) and their binary mixtures with NAP (b). The solid red lines represent VFT fits. The left and right insets of panel (b) present the dependence of T_g (BDS) of the NAP−acSACCH mixture on T_g and M_w of neat acSACCH, respectively.

again toward higher f, which means the end of the crystallization process.

From Figure 1, one can also observe that the degree of API crystallization in NAP−acMAL, NAP−acRAF, and NAP−acSTA systems depends on the molecular weight (M_w) of the acetylated saccharide. This phenomenon, which can be monitored by the change in the amplitude of the structural relaxation, is most noticeable for the mixture of NAP with acMAL. Note that in this SD, both components, API and the modified saccharide, crystallize at higher T (as shown in Figure 1a, the lowering amplitude of the α-process at 339 and 343 K indicates the crystallization of NAP, while the significant decrease in the amplitude at 355 K points to the crystallization of acMAL). Importantly, in the case of the NAP−ac-α-CD, 1:1 m/m SD (panel d of Figure 1), the crystallization does not occur. This mixture (as concluded from our preliminary studies), in contrast to other binary systems, is stable in the whole measured T range.

To characterize the molecular dynamics of the studied 1:1 m/m binary systems, the spectra presented in Figure 1 were fitted to the Havriliak−Negami (HN)[41] function, taking into account the DC contribution

$$\varepsilon(\bar{\omega})'' = \frac{\sigma_{DC}}{\varepsilon_0 \bar{\omega}} + \varepsilon_\infty + \frac{\Delta\varepsilon}{[1 + (i\bar{\omega}\tau_{HN})^\alpha]^\gamma} \quad (1)$$

where α and γ are the shape parameters, describing the slopes of the high- and low-frequency part of a given relaxation process, respectively, $\Delta\varepsilon$ is the dielectric relaxation strength, τ_{HN} is the HN relaxation time, ε_0 is the vacuum permittivity, and $\bar{\omega}$ is an angular frequency ($\bar{\omega} = 2\pi f$). Afterward, using the formula given in a book edited by Kremer and Schönhals,[42] the structural relaxation times (τ_α) have been recalculated from τ_{HN}. Subsequently, τ_α was plotted *versus* reciprocal temperature (Figure 2b) and compiled with analogous data determined for neat acSACCHs (Figure 2a).[39] Next, to describe the temperature dependencies of τ_α, the Vogel−Fulcher−Tammann (VFT)[43−45] equation (Figure 2, solid red lines) was applied

$$\tau_\alpha = \tau_{VFT} \exp\left(\frac{D_T T_0}{T - T_0}\right) \quad (2)$$

in which τ_{VFT} is the time scale of vibrational motions and D_T is the strength parameter, while T_0 represents the temperature at which τ_α tends to infinity. Obtained fits were used to determine the values of T_g (defined as a T at which α-relaxation times reach 100 s) for each binary system. As can be observed in Figure 2, the glass transition temperatures calculated for the examined SDs are lower with respect to T_g of neat modified saccharides.[39] Moreover, they generally increase linearly with increasing M_w of the used EXC (although the T_g of NAP−acMAL and NAP−acRAF, 1:1 m/m systems is practically the same); see the right inset of Figure 2b. It can also be noticed that there is a clear dependence between the T_g of the NAP−acSACCH mixture and T_g of neat acSACCH, that is, higher T_g of the former is accompanied by higher T_g of the latter; see the left inset of Figure 2b.

It should be noted that the glass transition temperatures obtained from BDS measurements for the considered SDs are additionally given in Table 1. In this table, we also included the values of this parameter determined from DSC experiments carried out at various heating rates, ϕ (results of these investigations will be described and discussed in detail later on). As illustrated, there is quite good correspondence between the T_g obtained from dielectric and calorimetric (ϕ = 10 K/min) studies for each examined binary mixture.

Table 1. Values of T_g Determined from Dielectric Measurements and T_g and Temperatures of the Crystallization Process (T_p, T_o) Obtained from DSC Thermograms Measured at Different Heating Rates

binary mixture in 1:1 m/m ratio	ϕ [K/min]	T_g^{BDS} [K] ±0.1 K	T_g^{DSC} [K] ±0.1 K	T_p [K] ±0.1 K	T_o [K] ±0.1 K
NAP−acMAL	2.5		299.1	359.0	354.1
	5		301.4	368.2	360.4
	7.5		301.9	375.5	365.5
	10	299.2	303.2	381.4	368.2
NAP−acRAF	5		299.1	360.2	352.5
	10	298.7	300.5	367.2	358.1
	15		301.7	370.9	359.5
	20		302.1	373.5	360.5
NAP−acSTA	2.5		304.8	366.1	356.4
	5		306.4	374.5	361.1
	7.5		307.1	377.7	364.6
	10	313.5	309.1		
NAP−ac-α-CD	2.5		342.1		
	10	341.5	346.1		

https://dx.doi.org/10.1021/acs.molpharmaceut.0c00982
Mol. Pharmaceutics 2021, 18, 347−358

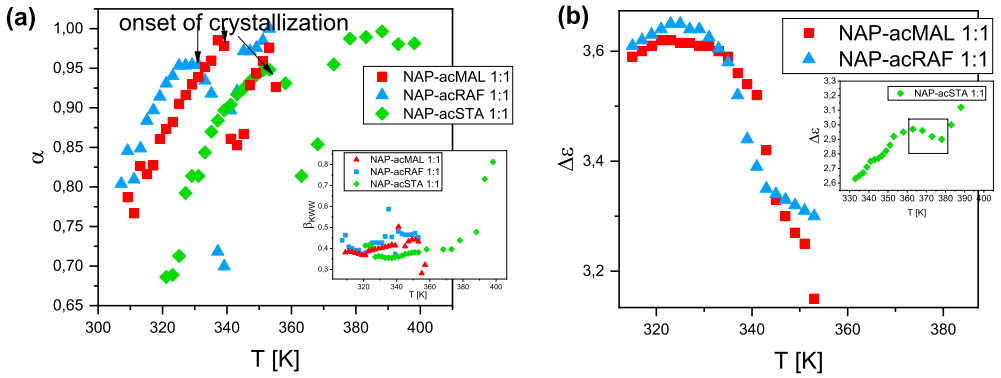

Figure 3. Temperature dependencies of the α parameter obtained from the HN function (eq 1) and Kohlrausch−Williams−Watts exponent, β_{KWW} (inset) (a). The changes in dielectric strength of the α-process ($\Delta\varepsilon$) with temperature for 1:1 m/m mixtures of NAP with acMAL and acRAF (b). The inset shows the analogous data for the equimolar NAP−acSTA SD.

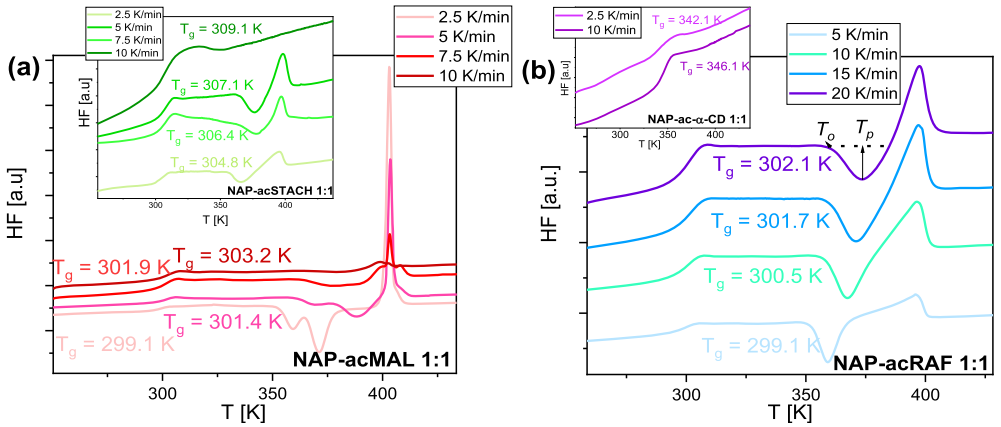

Figure 4. DSC curves obtained for binary mixtures of NAP with acMAL (a), acRAF (b), acSTA (inset of panel a), and ac-α-CD (inset of panel b), 1:1 m/m. Thermograms were measured with the indicated heating rates.

What is more, for the three of the studied equimolar binary systems (NAP−acMAL, NAP−acRAF, and NAP−acSTA), we performed additional analysis to check how the parameters describing the structural (α)-relaxation process change in the temperature ranges where the crystallization is observed in dielectric spectra. In Figure 3, two of them obtained directly from the HN fits, that is, α and $\Delta\varepsilon$—see eq 1 and the stretched/Kohlrausch−Williams−Watts exponent (β_{KWW}), calculated using the following formula:[46]

$$\alpha\gamma = \beta_{KWW}^{1.23} \quad (3)$$

where γ is the second (after α) shape parameter in the HN function, presented as a function of temperature. As illustrated in Figure 3a, in each case, there is a nonmonotonic behavior of α and β_{KWW}. In particular, the increase in α with increasing T is interrupted by a sharp decrease at temperature at which the samples start to crystallize; see Figure 1. Moreover, in a similar T range, some variations are visible in the dependences β_{KWW} *versus* T. The third manifestation of the ongoing crystallization process in the considered binary mixtures is the decrease in dielectric strength of the α-process ($\Delta\varepsilon$), observed in Figure 3b.

Subsequently, having in mind that NAP recrystallizes in three of the examined equimolar binary mixtures (NAP−acMAL, NAP−acRAF, and NAP−acSTA, 1:1 SDs), we carried out nonisothermal calorimetric measurements to calculate the activation barrier of crystallization in these systems. Thermograms measured with various heating rates (ϕ) for each sample are presented in Figure 4 (panels a and b). Additionally, in the inset of Figure 4b, we included two representative DSC curves determined for the NAP−ac-α-CD, 1:1 SD (noncrystallizing system). As can be seen, there are two endothermic processes in the thermograms collected for the mixtures of NAP with three linear acetylated carbohydrates. The first one, appearing at lower T, is related to the glass transition phenomenon, whereas the second one is associated with the melting of the crystalline sample. Moreover, at some ϕ, one can notice the presence of one or two (NAP−acMAL SD) exothermic events, indicating the cold crystallization. Note that with the increasing heating rate, both the first endothermic peak and exothermic peak (or peaks in the case of the NAP−acMAL SD) are shifting toward higher temperatures in the examined binary systems.

It is worth pointing out that for NAP−acMAL (panel a in Figure 4) and NAP−acRAF (panel b in Figure 4) systems, the crystallization process occurs independently of ϕ. For the NAP−acSTA SD (the inset of panel a in Figure 4), this phenomenon can be detected at the heating rates from 2.5 to 7.5 K/min. In turn, in the case of the NAP−ac-α-CD system (inset of panel b in Figure 4), there is no sign of crystallization in DSC curves measured with various ϕ, which is consistent with the results of dielectric investigations. It should be added that the presence of two exothermic events in DSC curves measured for the NAP−acMAL SD is related to the crystallization of both components of the mixture (API and

https://dx.doi.org/10.1021/acs.molpharmaceut.0c00982
Mol. Pharmaceutics 2021, 18, 347−358

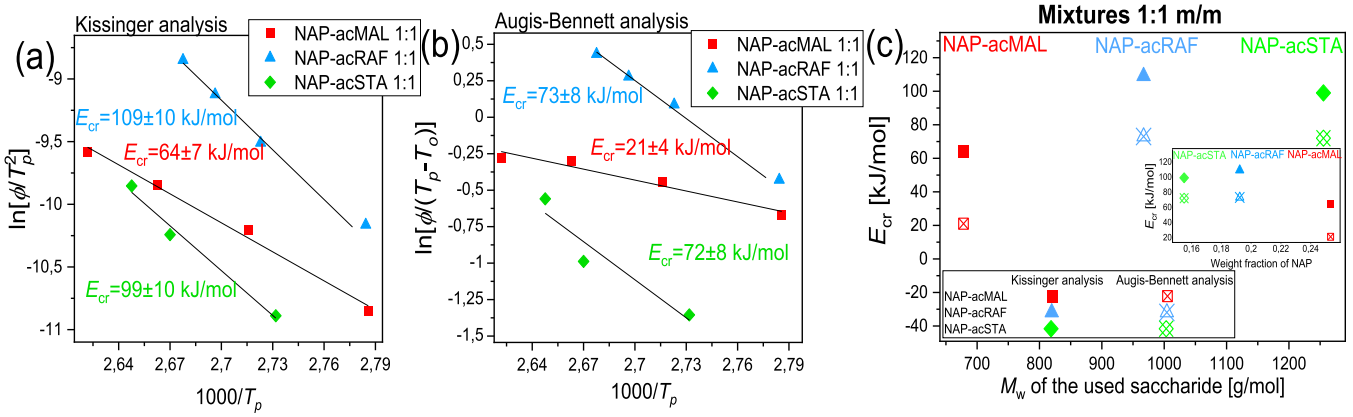

Figure 5. Kissinger (a) and Augis and Bennett (b) plots for exothermic crystallization peaks in NAP−acMAL, NAP−acRAF, and NAP−acSTA binary mixtures (1:1 m/m), characterized by temperatures given in Table 1. The solid black lines represent the linear fits to eqs 4 and 5. The values of crystallization energy (E_{cr}) calculated from both analyses plotted *versus* M_w of the saccharide used for the preparation of binary systems (c). The inset of panel (c) presents the dependence of E_{cr} on the weight fraction of NAP in three examined equimolar mixtures.

modified saccharide). Taking into account the results of previous BDS studies and additional XRD measurements (Figure 6 described later on), it can be stated that exothermic peaks occurring in thermograms of NAP−acMAL systems at lower and higher T are associated with the crystallization of the API and acMAL, respectively.

Afterward, from the analysis of thermograms presented in Figure 4, the activation energy of nonisothermal crystallization (E_{cr}) for equimolar binary mixtures of NAP with linear acSACCHs was calculated. For this purpose, we used the Kissinger method,[47] which relies on the analysis of the variation in the peak temperature of crystallization (T_p)

$$\ln\left(\frac{\phi}{T_p^2}\right) = C_K - \frac{E_{cr}}{RT_p} \tag{4}$$

and Augis−Bennett approach[48] that takes into account the onset temperature of crystallization, T_o

$$\ln\left(\frac{\phi}{T_p - T_0}\right) = C_{AG} - \frac{E_{cr}}{RT_p} \tag{5}$$

C_K in eq 4 and C_{AG} in eq 5 are fitting parameters. It should be mentioned that in the case of the NAP−acMAL mixture, the first exothermic peak visible in thermograms (assigned to the recrystallization of the API) was taken for the calculations. The results of both analyses together with the obtained activation energies are presented in Figure 5a,b (note that the values of T_p, T_o and applied heating rates (ϕ) are included in Table 1). As can be seen, for each binary system, the value of E_{cr} calculated from the Kissinger approach is significantly higher with respect to that determined from the Augis−Bennett expression. Such differences are well visualized in panel c of Figure 5 and in the inset of this figure, where the obtained activation energies have been presented as a function of M_w of the used, modified carbohydrate and the weight fraction of NAP. Essentially, one can observe that E_{cr} increases with the increasing molecular weight of the acSACCH and simultaneously with the decreasing content of the API in the mixture (negative correlation). However, it should be stressed that in the case of the SDs with acRAF and acSTA, despite various M_ws of these carbohydrates, the values of E_{cr} are comparable.

What is more, we also performed additional nonisothermal DSC measurements for NAP−acSACCH binary mixtures with the same content of APIs in each sample (1:5.45 weight ratio, which corresponds to the following molar ratios: 1:1 (NAP−acSTA), 1:1.3 (NAP−acRAF), and 1:1.85 (NAP−acMAL)). The obtained thermograms (except for those collected for the NAP−acSTA system, which are identical with DSC curves shown in the inset of Figure 4a) and results of the analysis carried out with the use of Kissinger and Augis−Bennett methods (eqs 4 and 5) are illustrated in the Supporting Information, Figures S1 and S2. As can be seen, the value of E_{cr} from both approaches is the greatest for the SD with acSTA (it exceeds that calculated for the NAP−acRAF 1:5.45 SD). Note that a high value of E_{cr} for the NAP−acMAL system is not entirely reliable because in this mixture, in contrast to the equimolar one (1:1 m/m), there is a contribution from both crystallizing components to the overall crystallization (only one broad exothermic peak in thermograms presented in Figure S1). Consequently, the estimation of E_{cr} of the API is hardly possible. Herein, it should also be noted that irrespectively of the heating rate, NAP always crystallized from binary mixtures with acMAL and acRAF, while in the case of acSTA, at higher ϕ, the API crystallization was suppressed and not detected in the measured thermograms.

Nevertheless, it must be emphasized that while probing the impact of various kinds of EXCs differing in molecular weight on the crystallization ability of labile amorphous APIs, the collected data should be first normalized and discussed with respect to the molar not the weight ratio. The molar ratio is a reference point allowing us to compare the activity against the crystallization of the selected matrices. Application of the protocol relying on measuring the SD of varying weight ratios seems to be reasonable only in the case of systems composed of APIs and exclusively one EXC (with different concentrations). The change in the crystallization pattern is a natural consequence of varying molar concentrations in binary mixtures.

Having BDS and DSC data measured, we performed XRD studies to verify the phase composition and crystallization tendency of binary mixtures and to identify the crystalline forms of their components. The measurements for SDs were carried out after their recrystallization (1 day after). It should be noted that XRD experiments performed immediately after

https://dx.doi.org/10.1021/acs.molpharmaceut.0c00982
Mol. Pharmaceutics 2021, 18, 347−358

the supercooling of liquids showed that the fresh binary mixtures were amorphous; see Figure S3 in the Supporting Information. The crystal structure of neat NAP (diffraction data marked with a dotted line in Figure 6) was identified to be

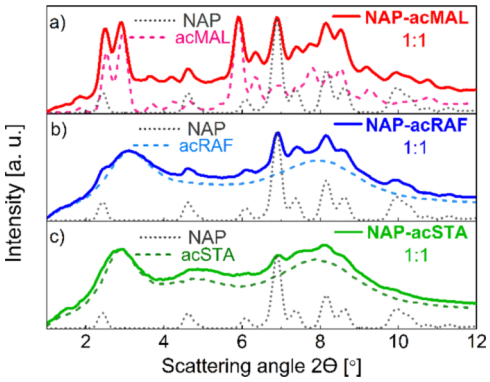

Figure 6. X-ray diffraction patterns for recrystallized equimolar mixtures of NAP with acMAL (a), acRAF (b), and acSTA (c) together with diffractograms measured for the crystalline NAP and neat modified saccharides.

composed of one polymorphic form that can be indexed in the P 1 21 1 space group symmetry with unit cell parameters $a \approx 7.73$ Å, $b \approx 5.72$ Å, and $c \approx 13.36$ Å and cell angles $\alpha \approx 90°$, $\beta \approx 93.7°$, and $\gamma \approx 90°$, according to the Crystallography Open Database (CCDC code: 735269). In all the measured binary mixtures of NAP with acSACCHs, there is a clear indication of recrystallization of APIs to the same polymorphic form, visible as the presence of sharp peaks at positions corresponding to the maxima of neat NAP. The structure of acRAF and acSTA in the mixtures with NAP is noncrystalline and show diffraction pattern typical for disordered materials, with two or three broad diffraction maxima, respectively, in the range up to 12°. In turn, acMAL recrystallizes in the mixture to the same crystalline form as in the case of neat acMAL, as evidenced by the positions of the observed Bragg peaks. Moreover, from the comparison of the intensity of NAP Bragg peaks in the SDs of the same molar ratio (1:1), it is clearly seen that the degree of crystallinity of NAP in the NAP−acMAL system is significantly higher than that in the mixtures with acRAF and acSTA. For the latter two systems, the recrystallization of NAP progresses much slower, wherein the slowest recrystallization is observed for the SD with acSTA, which is the saccharide with the highest molecular weight.

Summarizing this part of our work, one can state that the progress of crystallization of NAP in binary mixtures depends on the length of the saccharide chain (M_w). It is just mentioned that the API did not crystallize at the higher heating rate (10 K/min) in the system composed of acSTA. Moreover, for this SD, the activation barrier for the crystallization of NAP

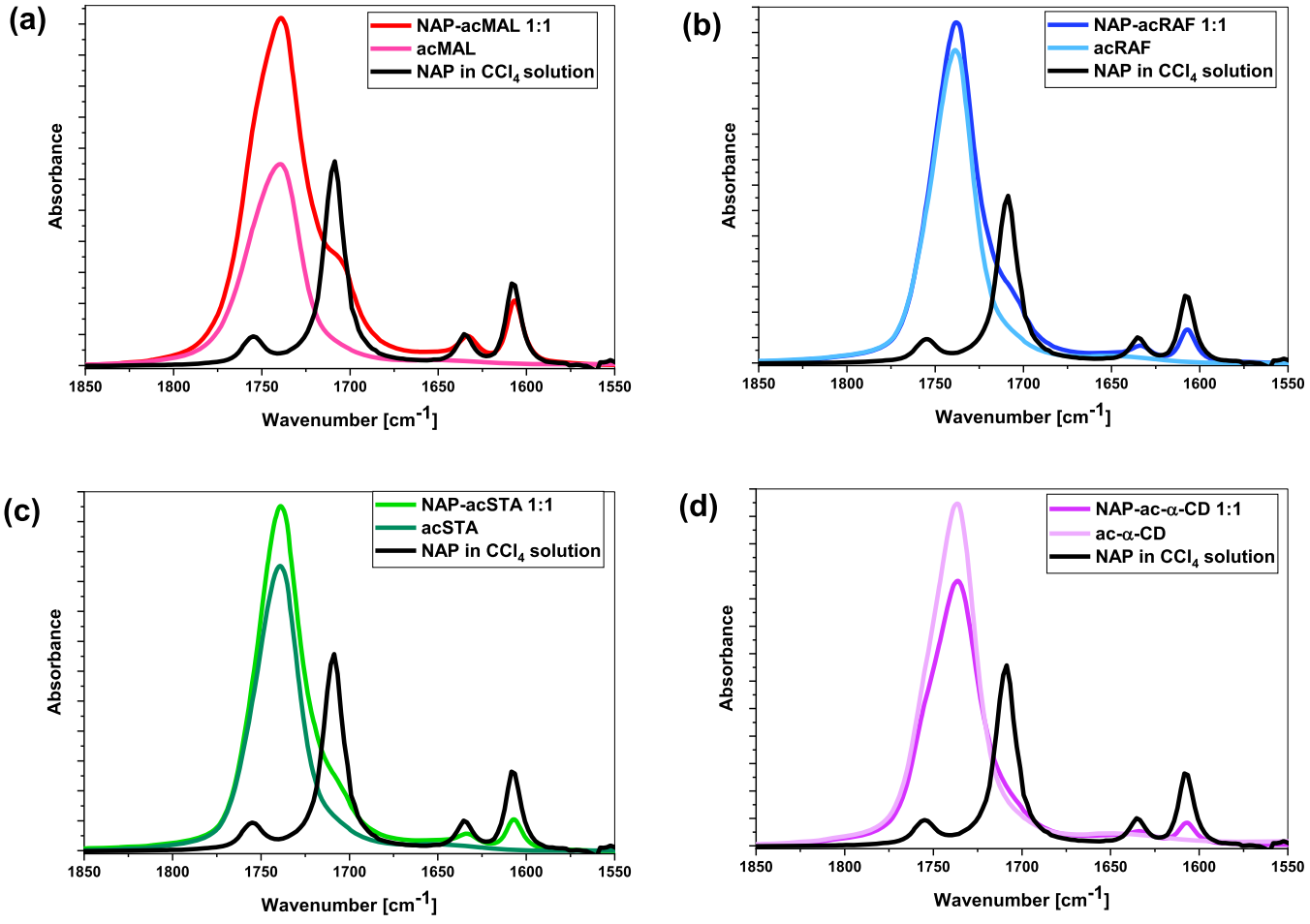

Figure 7. Infrared spectra of NAP in CCl_4 solution, supercooled acSACCHs, and NAP−acSACCH (1:1 m/m) binary mixtures in the range of 1850−1550 cm^{-1}.

https://dx.doi.org/10.1021/acs.molpharmaceut.0c00982
Mol. Pharmaceutics 2021, 18, 347−358

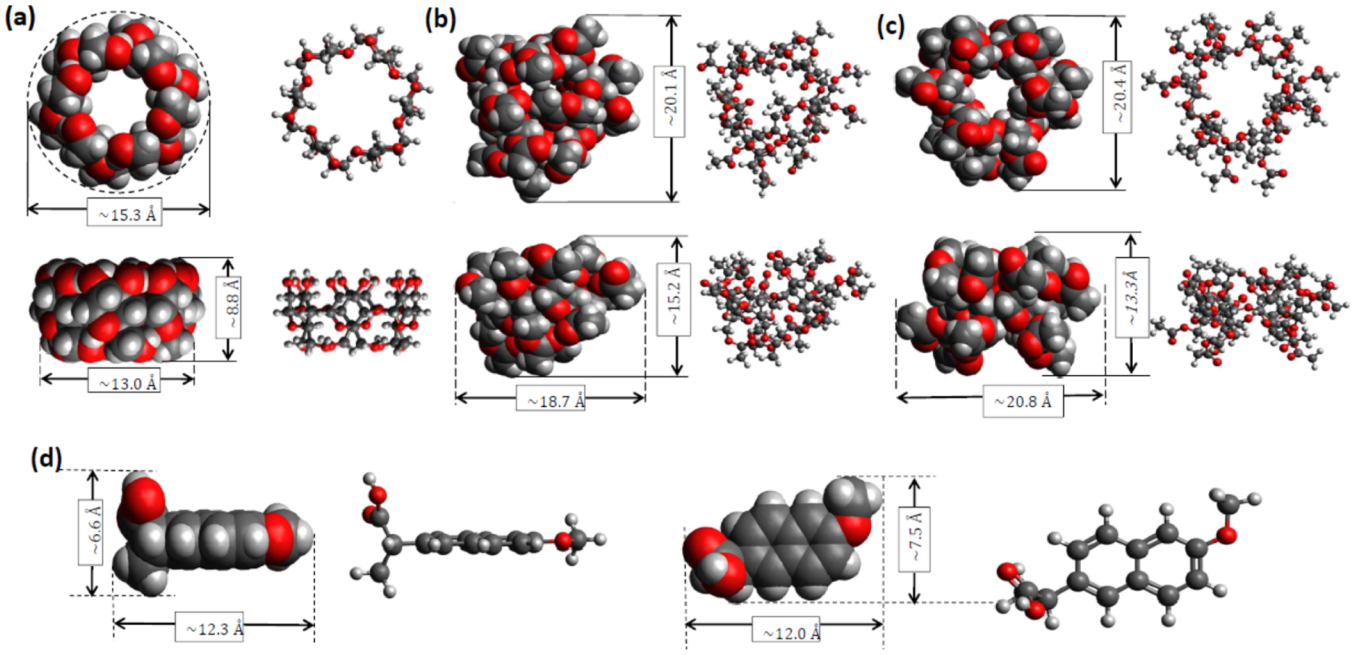

Figure 8. Molecular structure of isolated α-CD (a), acetyl-α-CD molecules (b,c—two conformers), and NAP, S-form (d) fully optimized by DFT.

is very high (a comparable E_{cr} was estimated only for the binary mixture with acRAF). On the other hand, the most remarkable finding is related to the complete suppression of the crystallization of the API in the NAP−ac-α-CD SD. For this mixture, NAP did not tend to crystallize irrespectively of the heating/cooling rate and concentration. To address and understand these interesting findings, we have carried out further FTIR measurements and DFT calculations to (i) determine the strength of interactions between both components of the mixtures and (ii) verify whether NAP may penetrate into the cavity formed by modified α-cyclodextrin and if this phenomenon is responsible for the lower crystallization ability of the active substance.

Infrared studies of the individual components and NAP−acSACCH (1:1 m/m) SDs were performed at room temperature. FTIR spectra of the crystalline NAP and NAP diluted in a CCl_4 liquid mixture (frequency range from 3600 to 950 cm^{-1}), collected to better visualize the interactions between API molecules, are shown in Figure S4 in the Supporting Information. Additionally, in Figures S5−S8, the comparison of the spectra of NAP in CCl_4 solution and supercooled acSACCHs (acMAL, acRAF, acSTA, and ac-α-CD) and their binary mixtures with NAP (1:1 m/m), measured in the 3700−2400 and 1850−950 cm^{-1} regions, is depicted. The same data, presented in the narrower frequency range, that is, 1850−1550 cm^{-1}, are presented in Figure 7.

Herein, it should be mentioned that CCl_4, as an inert solvent, was used as a reference to obtain the information about the extent of aggregation of NAP. The measurement of the IR spectrum of APIs diluted in CCl_4 (Figure S4) shows that NAP molecules exist as H-bonded dimers under such conditions. Interestingly, the band profile of the OH stretching vibrations for NAP in the SDs looks similar to that found in CCl_4 solution. Hence, this simple experiment, commonly applied to gain insights into the H-bond pattern, allowed us to certify that API chains connected via H-bonds (a characteristic feature of NAP in crystals) are being destroyed in binary mixtures with acetylated saccharides. In these systems, NAP exists as dimers; for details, see the Supporting Information.

Comparing the IR spectra of NAP in CCl_4 solution with those of neat acSACCHs and NAP−acSACCH SDs (Figures S5−S8), it is interesting to find some important spectral features, especially in two regions: 3100−3400 and 1550−1850 cm^{-1}. An additional broad band of low intensity is detected for all binary systems in the range of 3100−3400 cm^{-1}, which suggests some kind of an association process between NAP molecules or between NAP and modified saccharides at room temperature. In each examined mixture, the position of this new band is comparable (NAP−ac-α-CD: 3633 cm^{-1}, NAP−acMAL: 3634 cm^{-1}, NAP−acRAF: 3633 cm^{-1}, and NAP−acSTA: 3635 cm^{-1}). The significant changes in the band profile occur in the frequency range of 1550−1850 cm^{-1}. As shown in Figure 7, all NAP−acSACCH SDs exhibit an additional shoulder in the C═O band profile at about 1705 cm^{-1}, which is absent for neat modified carbohydrates. Moreover, there are no bands in the range of 1550−1650 cm^{-1} in the IR spectra of the studied EXCs. In the case of binary mixtures, there are two additional peaks in this region (1634 and 1607 cm^{-1}), analogous to those in NAP in CCl_4 solution (1635 and 1608 cm^{-1}). All these characteristic spectral features described above indicate that there are mainly H-bond interactions between API molecules in the considered binary mixtures. Although we cannot rule out that there might be some direct intermolecular interactions between NAP and modified saccharides, but even though it is the case, they are of a weak character.

As a final point, we carried out DFT calculations to check the compatibility between NAP dimers and the cavity in the ac-α-CD; see Figure 8. It is worth mentioning that there are numerous reports indicating that the native α-cyclodextrin can serve as a host for small compounds (namely, the API molecule might be closed inside the hydrophobic cavity in this saccharide[49−51]). In this context, one can refer to the work by Bettinetti et al.,[51] where it was shown that because of interactions between NAP and α-CD, the inclusion complex

https://dx.doi.org/10.1021/acs.molpharmaceut.0c00982
Mol. Pharmaceutics 2021, 18, 347−358

stabilizing the amorphous pharmaceutical can be formed. Note that the authors also indicated that a somewhat different so-called pseudo-inclusion complex is created between this API and a noncyclic analogue of α-CD, that is, maltohexaose, M6 (the similar situation is less likely but probable in the case of the lower homologues of M6, such as maltotetraose, M4, or maltotriose, M3, revealing small complexing properties). The results of our computations, showing that dimers of NAP might be entrapped by α-CD, confirm the conclusions presented in ref 51. In turn, a completely different situation was found for the acetyl derivative of this carbohydrate (ac-α-CD). It turned out that acetyl moieties are highly mobile, leading to the formation of different conformers and strong modification of the chemical structure and properties of the cavity of α-CD. In Figure 8, we presented two representative conformations of the cyclic modified saccharide characterized by the higher (cavity is preserved) and lower (cavity is closed) energy. Interestingly, even in the case of the first molecular configuration, docking of the NAP dimers inside the saccharide is strongly suppressed because of the hindrance posed by acetyl units that reduce the size of the torus. On the other hand, the encapsulation of NAP is impossible for the second molecular conformation because the cavity is completely closed.

To elaborate on this issue in more detail, we also performed additional computations of the FTIR spectra of the equimolar systems composed of ac-α-CD and NAP located outside or inside the cavity formed by cyclic modified saccharide (data not shown). However, it was found that the vibration profiles of both systems are not so much different. Therefore, elucidation or discrimination which scenario is more probable based on the Fourier-transform infrared spectra supported by theoretical computations is not possible. At the moment, we can conclude that taking into account the energies of binary mixtures composed of NAP inside and outside the cavity (differing by up to 80 kJ/mol), the latter state seems to be more preferred. Herein, it should also be recalled that according to Bettinetti et al.,[51] the linear native oligosaccharide M6 (six glucose units) can be a supermolecule for NAP and form the pseudo-inclusion complex with this API. Hence, one could consider a similar scenario for acMAL, acRAF, and acSTA. However, taking into account that (i) we studied modified carbohydrates characterized by much different intermolecular interactions with respect to the native ones, (ii) the smaller matrices (up to four monomeric units) were used, and (iii) FTIR data revealed lack or weak interactions between NAP and linear or cyclic saccharides, the formation of some kind of pseudo-inclusion complexes in examined binary mixtures is hardly possible.

Therefore, although our studies clearly indicated that the length of the chain and topology of the EXC play a pivotal role in suppressing crystallization of NAP, there must be other factors than intermolecular interactions or geometrical compatibility of the host and guest molecules that is responsible for this phenomenon. One can suppose that the variation in the structure of the saccharide induces some changes in the free volume, as it was suggested for the bicalutamide-PVP SDs.[52] The other possibility is related to strong dispersive van der Waals interactions that make it harder for APIs to form the nucleus and trigger the crystal growth. However, to better understand this finding and the molecular mechanism responsible for this, further studies are required.

CONCLUSIONS

In this work, we have carried out BDS, nonisothermal DSC, and XRD measurements on the binary mixtures composed of NAP and selected acetylated saccharides (linear and cyclic). Our purpose was to investigate the influence of the chain length and topology of the EXC on the crystallization tendency of the examined API. Interestingly, dielectric and structural studies performed on equimolar (1:1 m/m) binary systems showed that the degree of crystallinity of NAP depends on the M_w of the linear saccharide—it was the highest for the case of NAP−acMAL SD. On the other hand, the presence of cyclic modified hexasaccharide, ac-α-CD, prevents NAP crystallization (even in the molar ratio of 10:1, such a phase transition was not detected). Further nonisothermal calorimetric measurements (at various heating rates ϕ) and analyses of the obtained data using Kissinger and Augis−Bennett approaches revealed that the length of the saccharide chain (acMAL, acRAF, and acSTA) has, in fact, an impact on the progress and activation barrier for the crystallization. In this context, one can mention that NAP did not crystallize at the ϕ = 10 K/min in the mixture with the tetrasaccharide acSTA. Moreover, for this binary system, the activation barrier for the crystallization of the API was very high (comparable to that determined for the trisaccharide acRAF). To understand this finding and the suppression (irrespectively of the heating rate and concentration) of NAP crystallization in the SD with ac-α-CD, we performed additional FTIR measurements and DFT calculations. Infrared studies demonstrated that there are no or only weak H-bonding intermolecular interactions between the API and each examined acetylated oligosaccharide. On the other hand, theoretical calculations showed that the encapsulation of NAP dimers to the cavity of ac-α-CD is impossible or strongly inhibited irrespectively of the molecular conformation of the EXC. Based on abovementioned data, it was concluded that except the intermolecular interactions and geometrical compatibility of NAP and ac-α-CD molecules, probably, other factors (e.g., some variations in the free volume or strong dispersive van der Waals interactions) might be responsible for suppressing the API crystallization. Nevertheless, this issue is yet to be clarified in the future.

ASSOCIATED CONTENT

Supporting Information

The Supporting Information is available free of charge at https://pubs.acs.org/doi/10.1021/acs.molpharmaceut.0c00982.

DSC thermograms measured at different heating rates for NAP−acMAL and NAP−acRAF (1:5.45 w/w) binary mixtures, results of the analysis of calorimetric data using Kissinger and Augis−Bennett approaches, X-ray diffraction patterns for NAP−acSACCH (1:1 m/m) systems collected at 293 K just after supercooling liquids, and infrared spectra of crystalline NAP and NAP in CCl_4 solution, supercooled acSACCHs (acMAL, acRAF, acSTA, and ac-α-CD) and NAP−acSACCH 1:1 m/m binary systems, measured at room temperature in the frequency range from 3700 to 950 cm^{-1}, together with the detailed description of the obtained results (PDF)

https://dx.doi.org/10.1021/acs.molpharmaceut.0c00982
Mol. Pharmaceutics 2021, 18, 347−358

AUTHOR INFORMATION

Corresponding Authors

Aldona Minecka − *Department of Pharmacognosy and Phytochemistry, Faculty of Pharmaceutical Sciences in Sosnowiec, Medical University of Silesia in Katowice, 41-200 Sosnowiec, Poland;* orcid.org/0000-0001-5603-032X; Email: aldona.minecka@med.sum.edu.pl

Ewa Kamińska − *Department of Pharmacognosy and Phytochemistry, Faculty of Pharmaceutical Sciences in Sosnowiec, Medical University of Silesia in Katowice, 41-200 Sosnowiec, Poland;* orcid.org/0000-0001-9725-8654; Email: ekaminska@sum.edu.pl

Authors

Magdalena Tarnacka − *A. Chelkowski Institute of Physics, University of Silesia in Katowice, 41-500 Chorzow, Poland; Silesian Center for Education and Interdisciplinary Research, University of Silesia, 41-500 Chorzow, Poland;* orcid.org/0000-0002-9444-3114

Karolina Jurkiewicz − *A. Chelkowski Institute of Physics, University of Silesia in Katowice, 41-500 Chorzow, Poland; Silesian Center for Education and Interdisciplinary Research, University of Silesia, 41-500 Chorzow, Poland;* orcid.org/0000-0002-4289-7827

Barbara Hachuła − *Institute of Chemistry, University of Silesia, 40-006 Katowice, Poland*

Roman Wrzalik − *A. Chelkowski Institute of Physics, University of Silesia in Katowice, 41-500 Chorzow, Poland; Silesian Center for Education and Interdisciplinary Research, University of Silesia, 41-500 Chorzow, Poland*

Kamil Kamiński − *A. Chelkowski Institute of Physics, University of Silesia in Katowice, 41-500 Chorzow, Poland; Silesian Center for Education and Interdisciplinary Research, University of Silesia, 41-500 Chorzow, Poland;* orcid.org/0000-0002-5871-0203

Marian Paluch − *A. Chelkowski Institute of Physics, University of Silesia in Katowice, 41-500 Chorzow, Poland; Silesian Center for Education and Interdisciplinary Research, University of Silesia, 41-500 Chorzow, Poland*

Complete contact information is available at: https://pubs.acs.org/10.1021/acs.molpharmaceut.0c00982

Notes

The authors declare no competing financial interest.

ACKNOWLEDGMENTS

A.M. and E.K. are thankful for the financial support from the National Science Center within the framework of the Sonata BIS project (grant no. DEC-2016/22/E/NZ7/00266). K.J. is grateful for the financial support from the Foundation for Polish Science within the START program. The authors would like to thank P. Spychalska and A. Kasprzycka for the synthesis of acetylated oligosaccharides: acRAF, acSTA, and ac-α-CD.

REFERENCES

(1) Jones, D. *Pharmaceutical Applications of Polymers for Drug Delivery*; Smithers Rapra Publishing: United Kingdom, 2004; ISSN: 0899-3144.

(2) Karolewicz, B. A review of polymers as multifunctional excipients in drug dosage form technology. *Saudi Pharm. J.* **2016**, *24*, 525−536.

(3) Gandhi, K. J.; Deshmane, S. V.; Biyani, K. R. Polymers in pharmaceutical drug delivery system: a review. *Int. J. Pharm. Sci. Rev. Res.* **2012**, *14*, 57−66.

(4) Baghel, S.; Cathcart, H.; O'Reilly, N. J. Polymeric Amorphous Solid Dispersions: A Review of Amorphization, Crystallization, Stabilization, Solid-State Characterization, and Aqueous Solubilization of Biopharmaceutical Classification System Class II Drugs. *J. Pharm. Sci.* **2016**, *105*, 2527−2544.

(5) Qian, F.; Huang, J.; Hussain, M. A. Drug−Polymer Solubility and Miscibility: Stability Consideration and Practical Challenges in Amorphous Solid Dispersion Development. *J. Pharm. Sci.* **2010**, *99*, 2941−2947.

(6) Knapik, J.; Wojnarowska, Z.; Grzybowska, K.; Hawelek, L.; Sawicki, W.; Wlodarski, K.; Markowski, J.; Paluch, M. Physical stability of the amorphous anticholesterol agent (ezetimibe): the role of molecular mobility. *Mol. Pharm.* **2014**, *11*, 4280−4290.

(7) Knapik, J.; Wojnarowska, Z.; Grzybowska, K.; Tajber, L.; Mesallati, H.; Paluch, K. J.; Paluch, M. Molecular dynamics and physical stability of amorphous nimesulide drug and its binary drug-polymer systems. *Mol. Pharm.* **2016**, *13*, 1937−1946.

(8) Szczurek, J.; Rams-Baron, M.; Knapik-Kowalczuk, J.; Antosik, A.; Szafraniec, J.; Jamróz, W.; Dulski, M.; Jachowicz, R.; Paluch, M. Molecular dynamics, recrystallization behavior, and water solubility of the amorphous anticancer agent Bicalutamide and its Polyvinylpyrrolidone mixtures. *Mol. Pharm.* **2017**, *14*, 1071−1081.

(9) Chmiel, K.; Knapik-Kowalczuk, J.; Jurkiewicz, K.; Sawicki, W.; Jachowicz, R.; Paluch, M. A new method to identify physically stable concentration of amorphous solid dispersions (I): Case of Flutamide + Kollidon VA64. *Mol. Pharm.* **2017**, *14*, 3370−3380.

(10) Wlodarski, K.; Sawicki, W.; Haber, K.; Knapik, J.; Wojnarowska, Z.; Paluch, M.; Lepek, P.; Hawelek, L.; Tajber, L. Physicochemical properties of tadalafil solid dispersions - Impact of polymer on the apparent solubility and dissolution rate of tadalafil. *Eur. J. Pharm. Biopharm.* **2015**, *94*, 106−115.

(11) Frank, D. S.; Matzger, A. J. Probing the interplay between amorphous solid dispersion stability and polymer functionality. *Mol. Pharm.* **2018**, *15*, 2714−2720.

(12) Prudic, A.; Kleetz, T.; Korf, M.; Ji, Y.; Sadowski, G. Influence of copolymer composition on the phase behavior of solid dispersions. *Mol. Pharm.* **2014**, *11*, 4189−4198.

(13) Knopp, M. M.; Olesen, N. E.; Holm, P.; Langguth, P.; Holm, R.; Rades, T. Influence of polymer molecular weight on drug-polymer solubility: A comparison between experimentally determined solubility in PVP and prediction derived from solubility in monomer. *J. Pharm. Sci.* **2015**, *104*, 2905−2912.

(14) Caron, V.; Hu, Y.; Tajber, L.; Erxleben, A.; Corrigan, O. I.; McArdle, P.; Healy, A. M. Amorphous solid dispersions of Sulfonamide/Soluplus® and Sulfonamide/PVP prepared by ball milling. *AAPS PharmSciTech* **2013**, *14*, 464−474.

(15) Edinger, M.; Knopp, M. M.; Kerdoncuff, H.; Rantanen, J.; Rades, T.; Löbmann, K. Quantification of microwave-induced amorphization of celecoxib in PVP tablets using transmission Raman spectroscopy. *Eur. J. Pharm. Sci.* **2018**, *117*, 62−67.

(16) Gupta, P.; Kakumanu, V. K.; Bansal, A. K. Stability and Solubility of Celecoxib−PVP Amorphous Dispersions: A Molecular Perspective. *Pharm. Res.* **2004**, *21*, 1762−1769.

(17) Kothari, K.; Ragoonanan, V.; Suryanarayanan, R. The role of drug−polymer hydrogen bonding interactions on the molecular mobility and physical stability of nifedipine solid dispersions. *Mol. Pharm.* **2015**, *12*, 162−170.

(18) Nielsen, L. H.; Rades, T.; Müllertz, A. Stabilisation of amorphous furosemide increases the oral drug bioavailability in rats. *Int. J. Pharm.* **2015**, *490*, 334−340.

(19) Wyttenbach, N.; Kuentz, M. Glass-forming ability of compounds in marketed amorphous drug Products. *Eur. J. Pharm. Biopharm.* **2017**, *112*, 204−208.

(20) Kalepu, S.; Nekkanti, V. Insoluble drug delivery strategies: Review of recent advances and business prospects. *Acta Pharm. Sin. B* **2015**, *5*, 442−453.

(21) Vasconcelos, T.; Marques, S.; das Neves, J.; Sarmento, B. Amorphous solid dispersions: Rational selection of a manufacturing process. *Adv. Drug Delivery Rev.* **2016**, *100*, 85−101.

(22) Jensen, K. T.; Larsen, F. H.; Löbmann, K.; Rades, T.; Grohganz, H. Influence of variation in molar ratio on co-amorphous drug-amino acid systems. *Eur. J. Pharm. Biopharm.* **2016**, *107*, 32−39.
(23) Kasten, G.; Grohganz, H.; Rades, T.; Löbmann, K. Development of a screening method for coamorphous formulations of drugs and amino acids. *Eur. J. Pharm. Sci.* **2016**, *95*, 28−35.
(24) Laitinen, R.; Löbmann, K.; Grohganz, H.; Strachan, C.; Rades, T. Amino acids as co-amorphous excipients for simvastatin and glibenclamide: physical properties and stability. *Mol. Pharm.* **2014**, *11*, 2381−2389.
(25) Kasten, G.; Löbmann, K.; Grohganz, H.; Rades, T. Co-former selection for co-amorphous drug-amino acid formulations. *Int. J. Pharm.* **2019**, *557*, 366−373.
(26) Wu, W.; Löbmann, K.; Schnitzkewitz, J.; Knuhtsen, A.; Pedersen, D. S.; Rades, T.; Grohganz, H. Dipeptides as co-formers in co-amorphous systems. *Eur. J. Pharm. Biopharm.* **2019**, *134*, 68−76.
(27) Mishra, J.; Bohr, A.; Rades, T.; Grohganz, H.; Löbmann, K. Whey proteins as stabilizers in amorphous solid dispersions. *Eur. J. Pharm. Sci.* **2019**, *128*, 144−151.
(28) Wu, W.; Ueda, H.; Löbmann, K.; Rades, T.; Grohganz, H. Organic acids as co-formers for co-amorphous systems - Influence of variation in molar ratio on the physicochemical properties of the co-amorphous systems. *Eur. J. Pharm. Biopharm.* **2018**, *131*, 25−32.
(29) Beyer, A.; Grohganz, H.; Löbmann, K.; Rades, T.; Leopold, C. Multivariate quantification of the solid state phase composition of co-Amorphous Naproxen-Indomethacin. *Molecules* **2015**, *20*, 19571−19587.
(30) Knapik, J.; Wojnarowska, Z.; Grzybowska, K.; Jurkiewicz, K.; Tajber, L.; Paluch, M. Molecular dynamics and physical stability of coamorphous Ezetimib and Indapamide mixtures. *Mol. Pharm.* **2015**, *12*, 3610−3619.
(31) Allesø, M.; Chieng, N.; Rehder, S.; Rantanen, J.; Rades, T.; Aaltonen, J. Enhanced dissolution rate and synchronized release of drugs in binary systems through formulation: Amorphous naproxen-cimetidine mixtures prepared by mechanical activation. *J. Controlled Release* **2009**, *136*, 45−53.
(32) Kaminska, E.; Adrjanowicz, K.; Tarnacka, M.; Kolodziejczyk, K.; Dulski, M.; Mapesa, E. U.; Zakowiecki, D.; Hawelek, L.; Kaczmarczyk-Sedlak, I.; Kaminski, K. Impact of inter- and intramolecular interactions on the physical stability of indomethacin dispersed in acetylated saccharides. *Mol. Pharm.* **2014**, *11*, 2935−2947.
(33) Grzybowska, K.; Paluch, M.; Wlodarczyk, P.; Grzybowski, A.; Kaminski, K.; Hawelek, L.; Zakowiecki, D.; Kasprzycka, A.; Jankowska-Sumara, I. Enhancement of amorphous celecoxib stability by mixing it with octaacetylmaltose: the molecular dynamics study. *Mol. Pharm.* **2012**, *9*, 894−904.
(34) Kaminska, E.; Tarnacka, M.; Wlodarczyk, P.; Jurkiewicz, K.; Kolodziejczyk, K.; Dulski, M.; Haznar-Garbacz, D.; Hawelek, L.; Kaminski, K.; Wlodarczyk, A.; Paluch, M. Studying the impact of modified saccharides on the molecular dynamics and crystallization tendencies of model API Nifedipine. *Mol. Pharm.* **2015**, *12*, 3007−3019.
(35) Kaminska, E.; Adrjanowicz, K.; Kaminski, K.; Wlodarczyk, P.; Hawelek, L.; Kolodziejczyk, K.; Tarnacka, M.; Zakowiecki, D.; Kaczmarczyk-Sedlak, I.; Pilch, J.; Paluch, M. A new way of stabilization of furosemide upon cryogenic grinding by using acylated saccharides matrices. The role of hydrogen bonds in decomposition mechanism. *Mol. Pharm.* **2013**, *10*, 1824−1835.
(36) Kaminska, E.; Tarnacka, M.; Kolodziejczyk, K.; Dulski, M.; Zakowiecki, D.; Hawelek, L.; Adrjanowicz, K.; Zych, M.; Garbacz, G.; Kaminski, K. Impact of low molecular weight excipient octaacetylmaltose on the liquid crystalline ordering and molecular dynamics in the supercooled liquid and glassy state of itraconazole. *Eur. J. Pharm. Biopharm.* **2014**, *88*, 1094−1104.
(37) Kaminska, E.; Madejczyk, O.; Tarnacka, M.; Jurkiewicz, K.; Kaminski, K.; Paluch, M. Studying of crystal growth and overall crystallization of naproxen from binary mixtures. *Eur. J. Pharm. Biopharm.* **2017**, *113*, 75−87.
(38) Schammé, B.; Couvrat, N.; Tognetti, V.; Delbreilh, L.; Dupray, V.; Dargent, É.; Coquerel, G. Investigation of drug-excipient interactions in Biclotymol amorphous solid dispersions. *Mol. Pharm.* **2018**, *15*, 1112−1125.
(39) Heczko, D.; Kamińska, E.; Minecka, A.; Tarnacka, M.; Waliłko, P.; Kasprzycka, A.; Kamiński, K.; Paluch, M. Studies on the molecular dynamics of acetylated oligosaccharides of different topologies (linear versus cyclic). *Carbohydr. Polym.* **2019**, *206*, 273−280.
(40) Frisch, M. J.; Trucks, G. W.; Schlegel, H. B.; Scuseria, G. E.; Robb, M. A.; Cheeseman, J. R.; Montgomery, J. A., Jr.; Vreven, T.; Kudin, K. N.; Burant, J. C.; Millam, J. M.; Iyengar, S. S.; Tomasi, J.; Barone, V.; Mennucci, B.; Cossi, M.; Scalmani, G.; Rega, N.; Petersson, G. A.; Nakatsuji, H.; Hada, M.; Ehara, M.; Toyota, K.; Fukuda, R.; Hasegawa, J.; Ishida, M.; Nakajima, T.; Honda, Y.; Kitao, O.; Nakai, H.; Klene, M.; Li, X.; Knox, J. E.; Hratchian, H. P.; Cross, J. B.; Bakken, V.; Adamo, C.; Jaramillo, J.; Gomperts, R.; Stratmann, R. E.; Yazyev, O.; Austin, A. J.; Cammi, R.; Pomelli, C.; Ochterski, J. W.; Ayala, P. Y.; Morokuma, K.; Voth, G. A.; Salvador, P.; Dannenberg, J. J.; Zakrzewski, V. G.; Dapprich, S.; Daniels, A. D.; Strain, M. C.; Farkas, O.; Malick, D. K.; Rabuck, A. D.; Raghavachari, K.; Foresman, J. B.; Ortiz, J. V.; Cui, Q.; Baboul, A. G.; Clifford, S.; Cioslowski, J.; Stefanov, B. B.; Liu, G.; Liashenko, A.; Piskorz, P.; Komaromi, I.; Martin, R. L.; Fox, D. J.; Keith, T.; Al-Laham, M. A.; Peng, C. Y.; Nanayakkara, A.; Challacombe, M.; Gill, P. M. W.; Johnson, B.; Chen, W.; Wong, M. W.; Gonzalez, C.; Pople, J. A. *Gaussian 03*, Revision C.02; Gaussian, Inc.: Wallingford CT, 2004.
(41) Havriliak, S.; Negami, S. A complex plane analysis of α-dispersions in some polymer systems. *J. Polym. Sci., Part C: Polym. Lett.* **1966**, *14*, 99−117.
(42) Kremer, F.; Schönhals, A. *Broadband Dielectric Spectroscopy*; Springer: Berlin, 2003.
(43) Vogel, H. Das temperaturabhangigkeitgesetz der Viskosität von Flüssigkeiten. *Phys. Z.* **1921**, *22*, 645−646.
(44) Fulcher, G. S. Analysis of recent measurements of the viscosity of glasses. *J. Am. Ceram. Soc.* **1925**, *8*, 339−355.
(45) Tammann, G.; Hesse, W. Die Abhängigkeit der Viscosität von der Temperatur bie unterkühlten Flüssigkeiten. *Z. Anorg. Allg. Chem.* **1926**, *156*, 245−257.
(46) Alvarez, F.; Alegra, A.; Colmenero, J. Relationship between the time-domain Kohlrausch−Williams−Watts and frequency-domain Havriliak−Negami relaxation functions. *Phys. Rev. B: Condens. Matter Mater. Phys.* **1991**, *44*, 7306−7312.
(47) Kissinger, H. E. Variation of peak temperature with heating rate in differential thermal analysis. *J. Res. Natl. Bur. Stand.* **1956**, *57*, 217−221.
(48) Augis, J. A.; Bennett, J. E. Calculation of the Avrami parameters for heterogeneous solid state reactions using a modified the Kissinger method. *J. Therm. Anal.* **1978**, *13*, 283−292.
(49) Carneiro, S.; Costa Duarte, F. Í.; Heimfarth, L.; Siqueira Quintans, J.; Quintans-Júnior, L.; Veiga Júnior, V.; Neves de Lima, Á.; Neves de Lima, Á. A. Cyclodextrin−Drug Inclusion Complexes: In Vivo and In Vitro Approaches. *Int. J. Mol. Sci.* **2019**, *20*, 642.
(50) Otero-Espinar, F. J.; Torres-Labandeira, J. J.; Alvarez-Lorenzo, C.; Blanco-Méndez, J. Cyclodextrins in drug delivery systems. *J. Drug Delivery Sci. Technol.* **2010**, *20*, 289−301.
(51) Bettinetti, G.; Sorrenti, M.; Negri, A.; Setti, M.; Mura, P.; Melani, F. Interaction of naproxen with alpha-cyclodextrin and its noncyclic analog maltohexaose. *Pharm. Res.* **1999**, *16*, 689−694.
(52) Pacult, J.; Rams-Baron, M.; Chrząszcz, B.; Jachowicz, R.; Paluch, M. Effect of polymer chain length on the physical stability of amorphous drug−polymer blends at ambient pressure. *Mol. Pharm.* **2018**, *15*, 2807−2815.

https://dx.doi.org/10.1021/acs.molpharmaceut.0c00982
Mol. Pharmaceutics 2021, 18, 347−358